ELSEVIER

Journal of Structural Geology 27 (2005) 35–49

JOURNAL OF STRUCTURAL GEOLOGY

www.elsevier.com/locate/jsg

Development of strike-slip faults from dikes, Sequoia National Park, California

Matthew d'Alessio[a], Stephen J. Martel[b,*]

[a]*University of California, Berkeley, CA 94720, USA*
[b]*University of Hawaii, Honolulu, HI 96822, USA*

Received 24 September 2003; received in revised form 25 March 2004; accepted 8 June 2004
Available online 18 September 2004

Abstract

Faults several kilometers long near Pear Lake in Sequoia National Park, California nucleated on preexisting dikes weakened by closely-spaced échelon joints. These joints essentially parallel much more widely spaced regional joints. Fault nucleation by dike fracturing can explain how a nearly planar fault can grow to lengths of several kilometers or more. We suggest that opening mode fractures, including dikes, might serve more commonly as nuclei for faults than is generally appreciated. The longest fault in the study area, the Pear Lake fault, has a trace length of ~7 km and a maximum measured lateral separation of 86–98 m. A sharp decrease in slip occurs near the center of the trace of the Pear Lake fault where another fault branches from it. Mechanical analyses demonstrate that a sharp decrease in slip is expected where a fault branches. All the faults near Pear Lake show non-elliptical slip distributions. Based on our mechanical analyses, we infer that the observed slip distributions reflect a mechanical interaction among the faults. The geometry and distribution of structures that precede faulting (i.e. dikes and joints) control to a large extent the structure of a fault network and hence the ultimate slip distribution on faults in the network.

Keywords: Faults; Dikes; Mechanics; Slip; Sierra Nevada

1. Introduction

Fault geometry fundamentally constrains fault behavior. For example, the size of a fault dictates how much it can slip and the magnitude of the largest earthquake it can generate (Pollard and Segall, 1987). The shape of a fault partly governs the amount of slip, the slip distribution, and where slip might nucleate or terminate (Schultz, 1999). The processes by which faults acquire their size and shape are not well understood though, especially for faults large enough to generate damaging earthquakes. We present here a previously unrecognised process for how strike-slip faults in the crust acquire lengths of several kilometers or more.

Laboratory experiments four decades ago by Brace and Bombalakis (1963) drew attention to some key questions regarding how faults grow in a body under compression. Their study showed that straight slits in a plexiglass plate did not propagate in-plane as shear fractures when they slipped. Instead, secondary opening-mode fractures propagated from the slit tips. These fractures grew oblique to the slits along a surface normal to the local least compressive stress, and they grew only a short distance relative to the slit length before terminating. The experiments were essentially two-dimensional, but subsequent three-dimensional experiments by Adams and Sines (1978) produced analogous results. These findings lead to three key questions about how natural faults grow in the crust:

1. How do faults acquire lengths of many kilometers?
2. Do faults propagate in-plane as shear fractures?
3. Why are so many faults nearly planar if faults tend to propagate out-of-plane?

Segall and Pollard (1983) addressed the latter two questions in their study on nearly vertical strike-slip faults in granitic rock along Bear Creek in the Sierra Nevada,

* Corresponding author. Tel.: +1-808-956-7797; fax: +1-808-956-5154
E-mail address: smartel@hawaii.edu (S.J. Martel).

0191-8141/$ - see front matter © 2004 Published by Elsevier Ltd.
doi:10.1016/j.jsg.2004.06.013

California. The faults they examined strike east-northeast, parallel to the dominant local joints. The joints contain undeformed mineral assemblages of chlorite and epidote, whereas in the faults these assemblages are deformed. Near the ends of many faults, fractures a few centimeters to a few meters long strike about 30° counterclockwise to the faults; such fractures are absent near the ends of the joints. Based on these field observations and their earlier mechanical analyses (Segall and Pollard, 1980) they reasoned that the faults developed from the joints. They concluded that some joints, after they opened, subsequently slipped and became faults after the ambient principal stresses rotated. Mere slip along the joints would yield faults with trace lengths matching those of the joints. In the outcrops examined by Segall and Pollard, the maximum joint trace lengths are several tens of meters but some fault traces are hundreds of meters long. These longer faults have échelon segments linked either by cavities or by opening-mode fractures oblique to the faults. From this evidence they reasoned that the faults of Bear Creek grew longer than the joints as originally separate faults linked together. Subsequent field investigations have corroborated these interpretations (Martel et al., 1988; Martel, 1990; Bürgmann and Pollard, 1994).

The question has remained open as to whether strike-slip faults can acquire lengths of many kilometers by exploiting joints. Martel et al. (1988) and Martel (1990) addressed this issue in part. They documented that Bear Creek fault zones more than a kilometer long have segments several tens of meters long, similar to the trace length of long, nearby joints. This implies that the fault zones exploited joints even as the zones grew to lengths of several kilometers. Scholz (2002), however, raised a cautionary note as to whether this could be a general explanation for how long faults form, noting that "for general applicability the initial tensile fractures would have to be persistent enough to form the long fault systems observed". Although in the Sierra such systems do occur (e.g. Lockwood and Lydon, 1975; Pachell and Evans, 2002), long faults also exist where such joint systems are absent.

To explore how strike-slip faults grow in crystalline rock in the absence of joint systems that extend several kilometers long along fault strike, we investigated a series of faults in Sequoia National Park in California (Fig. 1). These faults are hosted in granitic rocks near Pear Lake where the exposures above treeline in the glaciated environs are excellent. Here we describe the faults and their slip distributions, analyze the mechanics of the slip distribution, relate the slip distributions to the fault network geometry, and describe how this long fault system initiated and developed. We find that the mechanism by which the Pear Lake fault grew dramatically impacted its geometry, which in turn controlled the distribution of slip between individual segments.

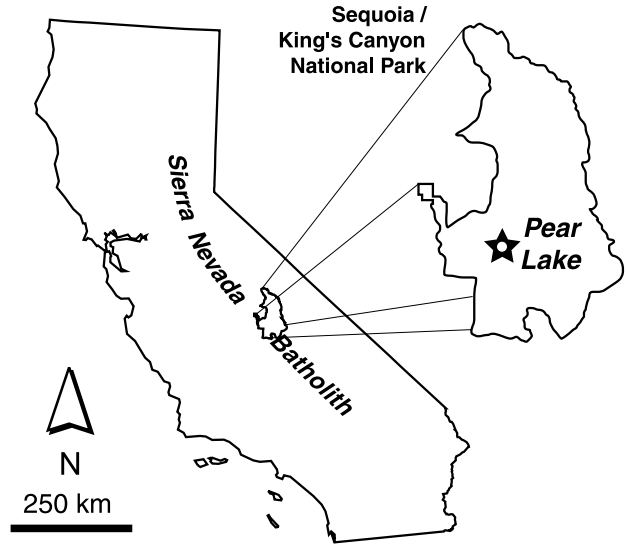

Fig. 1. Location of the Pear Lake region in Sequoia/King's Canyon National Park, California.

2. Geologic setting

2.1. Plutons

The faults near Pear Lake cut three main plutons (Fig. 2). From oldest to youngest, these are (a) the granite of Lodgepole Campground; (b) the granodiorite of Castle Creek; and (c) the Mitchell Peak Granodiorite. Within the area of Fig. 2, these plutons are coarse-grained, medium-grained, and fine-grained, respectively (Moore and Sisson, 1987). Stoped blocks of the granite of Lodgepole Campground occur in the granodiorite of Castle Creek (Fowler and Paterson, 1997), and stoped blocks of the granodiorite of Castle Creek in turn occur in the Mitchell Peak Granodiorite (Moore and Sisson, 1987). The respective U–Pb ages of these three plutons are (a) $\geq$115 Ma (Chen and Moore, 1982); (b) 98$\pm$2 Ma (Busby-Spera, 1983); and (c) 91 Ma (Chen and Moore, 1982). Geobarometric analyses (Chen and Moore, 1982; Ague and Brimhall, 1988) indicate that the two youngest plutons (and perhaps all three) probably were emplaced at a depth of 8–10 km (Fowler and Paterson, 1997). The plutons are elongate to the north-northwest and display a foliation that typically strikes north-northwest (Fowler and Paterson, 1997). Both the foliation and the pluton boundaries are cross-cut by faults near Pear Lake.

2.2. Shear zones

Steeply dipping ductile shear zones are perhaps the oldest planar structures near Pear Lake. These appear to be scarce, but are most noticeable between Pear Lake and Alta Peak (Fig. 2). The shear zones tend to be no more than a few centimeters thick, have traces no more than a few tens of meters long, and dip steeply. We observed strike-slip

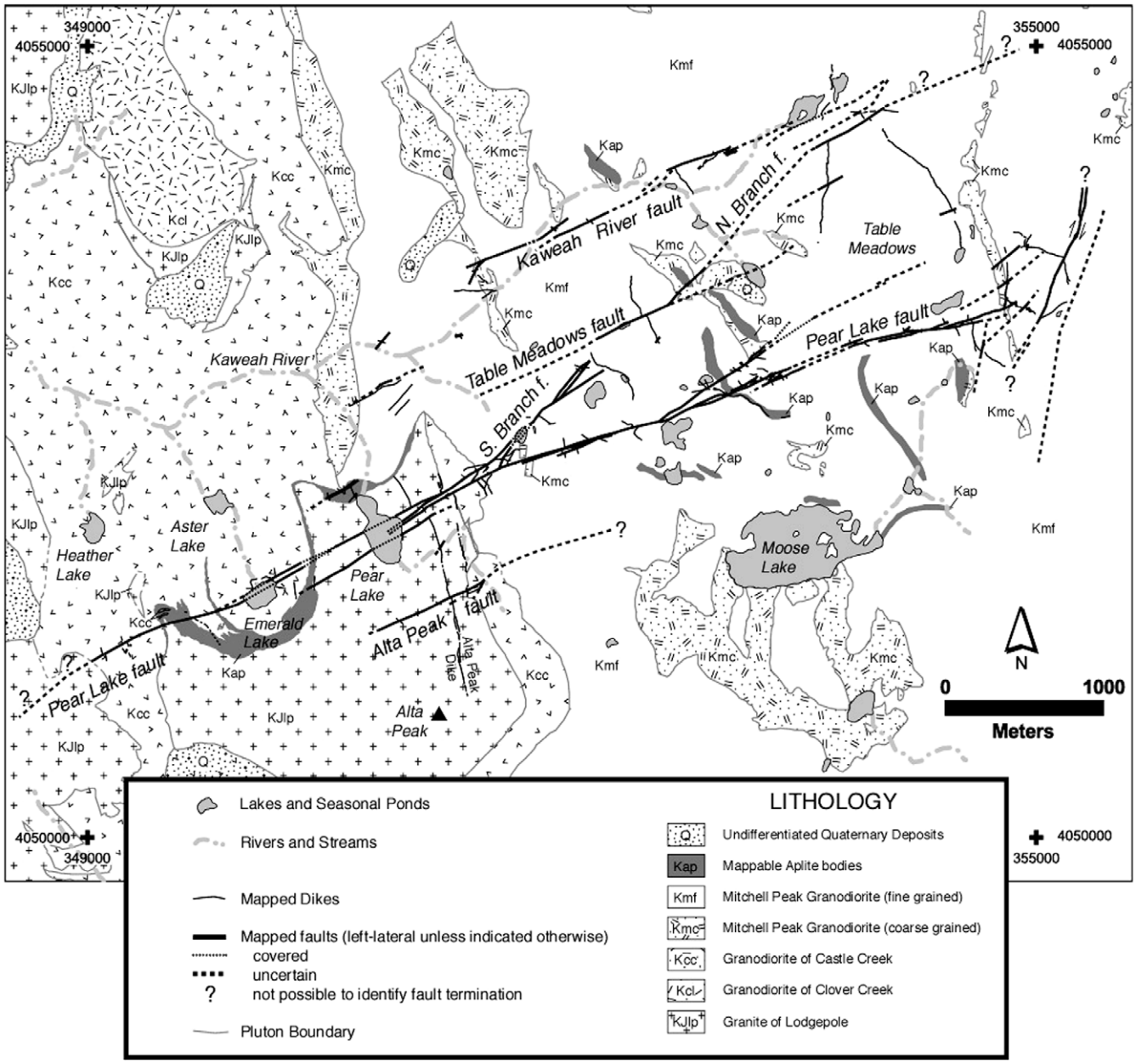

Fig. 2. Map of faults and plutons in the Pear lake study area. From oldest to youngest, the plutons are the granite of Lodgepole Campground (JKlp), the granodiorite of Castle Creek (Kcc), and the Mitchell Peak Granodiorite (Km). Pluton contacts are from Fowler and Paterson (1997). Coordinates are for UTM Zone 10 based on the North American Datum of 1983, with units of meters. The easternmost fault that strikes NNE was mapped by Moore and Sisson (1987); all other faults were mapped in this study.

separations as large as 55 cm along the shear zones. Right-lateral shear zones that strike ~N60E coexist with left-lateral shear zones that strike ~N14W. These are oblique to the faults that are the focus of our study.

2.3. Dikes

The oldest systematic, widespread structures we have identified near Pear Lake are steeply dipping dikes. We distinguish three main sets: mafic dikes that strike approximately north–south, aplite dikes that strike NW, and aplite dikes that strike ENE (Figs. 2–4). They commonly crop out along grassy strips and appear as prominent photolineaments (Fig. 3). The mafic dikes occur in a zone ~200 m wide within the eastern margin of the Lodgepole Campground pluton. The most prominent mafic dike is the westernmost. This dike is a key marker. It crops out ~200 m east of Pear Lake and extends towards Alta Peak; we refer to this as the Alta Peak dike. It has a maximum thickness of a few meters and can be traced for about 1 km. It is exposed over an elevation range of about 380 m. The dike is close to vertical, its dip ranging from 80°

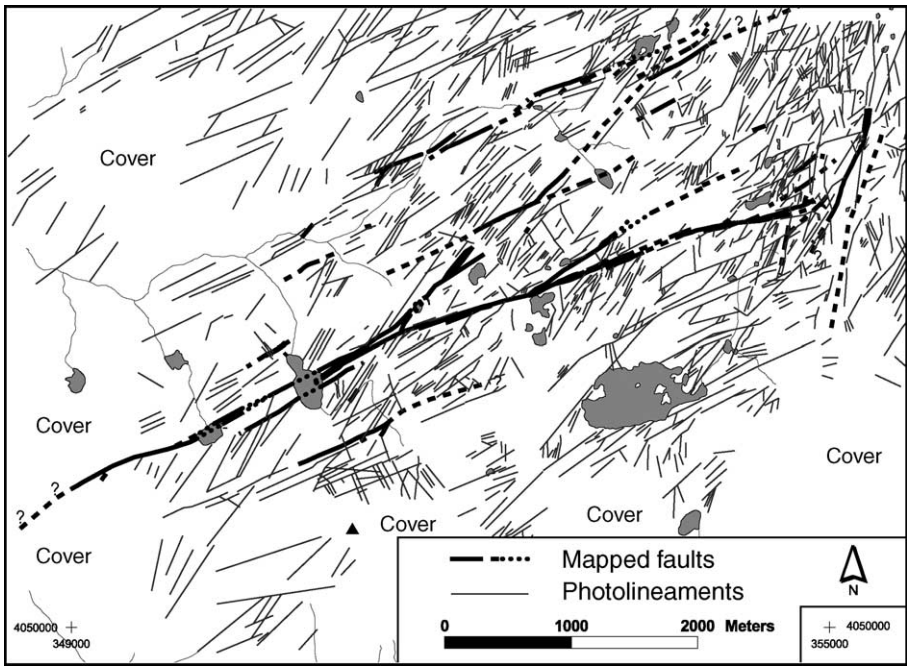

Fig. 3. Map of faults and photolineaments of the Pear Lake study area.

to the east to 78° to the west. Unlike the mafic dikes, the aplite dikes are distributed throughout the study area. They generally attain a maximum thickness of several decimeters, but some are a few meters thick. The edges of the aplite dikes are in sharp contact with the host rock. The NW-striking aplite dikes usually can be traced continuously for no more than a couple of hundred meters. Some aplite dikes that strike ENE can be traced along strike for more than 200 m and are exposed over an elevation range of at least 100 m (Fig. 5b). Aplite dikes that are either unfractured or mildly fractured cut older features but do not offset them left-laterally (Fig. 5c). This indicates that the dikes intruded as new opening mode fractures rather than intruding along preexisting left-lateral faults.

Direct evidence on the relative ages of the dike sets is scarce. Figure 5c shows an aplite dike striking ENE that appears to cut an aplite dike striking north, indicating that the ENE-striking dike is younger. We have not found definitive evidence as to the relative ages of the mafic dikes and the aplitic dikes, but the mafic dikes are confined to the oldest pluton and might be truncated by younger plutons (Moore and Sisson, 1987). The aplite dikes, in contrast, occur in all three plutons. We infer that the aplite dikes are younger than the mafic dikes, with the ENE-striking aplite dikes being the youngest.

2.4. Joints

North-northeast-striking joints are prominent near Pear Lake. These joints generally strike N25E–N35E (Fig. 4), are within a few degrees of vertical, and parallel prominent topographic lineaments (Figs. 3, 4 and 5a). Joint trace lengths typically are a few meters to a few tens of meters. The joints cut the aplite and mafic dikes and thus are younger than the dikes. The joints locally display fillings of chlorite.

The spacing of the joints varies in a systematic way. In the granite and granodiorite far from a dike, the spacing commonly is several meters. In contrast, within some dikes, especially within some ENE-striking aplite dikes, the joint spacing commonly is on the order of a few centimeters (Fig. 5d). Joints in the dikes typically form a band of échelon fractures and terminate at the dike margins, but some extend across the dikes into the host rock (Fig. 5d).

In contrast to the joint spacing, the joint orientation is fairly consistent. The joints typically dip steeply and strike N25E–N35E within the host rock, along the faults, and within the dikes, even though the orientation of dikes varies (Figs. 3, 4 and 6).

2.5. Faults

Faults with traces longer than 100 m are common near Pear Lake. The faults are expressed topographically as troughs, some more than 10 m wide and 10 m deep. The troughs typically are carpeted by grass along gentle slopes and filled by talus on steep slopes.

The longest and most prominent faults near Pear Lake strike N60E–N70E and dip steeply (Figs. 2 and 3). At least four have traces longer than 1 km. From north to south these are: the Kaweah River fault; the Table Meadows fault; the Pear Lake fault; and the Alta Peak fault. The longest is the Pear Lake fault, which is discussed separately below. Moore and Sisson (1987) mapped other ENE-striking faults

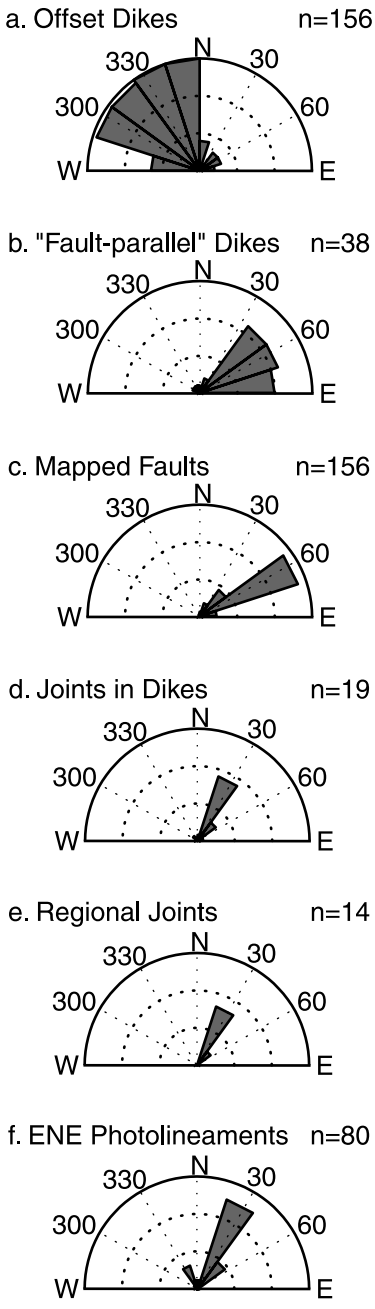

Fig. 4. Rose diagram showing strikes of various features. All features except those in (f) were measured in the field. (a) Offset dikes. (b) Dikes with strikes of NNE–ENE. (c) Faults. (d) Joints in dikes. (e) Joints. (f) ENE-striking photolineaments, interpreted to be regional joints (from aerial photographs).

hundreds of meters long within several kilometers of Pear Lake. The spacing between the primary fault traces on Fig. 2 ranges from about 0.5 to 1 km. The faults offset NW-striking aplite dikes and the Alta Peak dike left-laterally. These faults strike about 40° clockwise from the dominant joints (Figs. 4 and 5a) but are paralleled by aplite dikes (Figs. 5b and 6). No systematic regional joints parallel the ENE-striking faults near Pear Lake, in contrast to the structural style in the Bear Creek area as described by Bergbauer and Martel (1999). Another difference is that ENE-striking faults with trace lengths less than 100 m are scarce near Pear Lake but widespread at Bear Creek.

Two left-lateral faults strike ~N40E–N45E in the northeast quadrant of Fig. 2. Each has a trace length of 1–1.5 km. These faults branch from ENE-striking faults. The 'southern branch fault' extends from the Pear Lake fault towards the Table Meadows fault. The 'northern branch fault' connects the Table Meadows fault and the Kaweah River fault.

Two faults that strike N15E–N20E are located near the eastern edge of Fig. 2; their traces are spaced about 150 m apart. The western fault occurs along the western contact of a highly fractured, elongate body of chloritized rock several meters thick. We mapped this fault over a distance of about 1 km and measured right-lateral separations of 8.5 and 12.7 m along it. We could not find slickenlines on this fault but did observe steeply-plunging 'pull-apart' cavities between left-stepping strands of the fault, and we interpret those as indicating near-horizontal slip. Moore and Sisson (1987) mapped the 1.7-km-long trace of the eastern right-lateral fault. We did not determine the lateral separation across this fault, but given its proximity to the nearly-parallel western fault and their similar traces lengths, we expect the lateral separations would be similar.

3. The Pear Lake fault

Our investigation of fault formation, fault structure, and fault slip focused on the Pear Lake fault (Fig. 2). Its topographic expression extends for ~7 km, and offset dikes permit slip measurements over almost this entire distance. Troughs along the fault are exposed over an elevation range of about 500 m. They exceed 10 m in depth in several places and are spectacularly expressed as notches in the ridge west of Pear Lake (Fig. 5a). Deep troughs along the fault also extend through Pear Lake and Emerald Lake. The troughs range in width from 2.6 m to more than 10 m. Surprisingly, some of the narrowest stretches along the fault trough occur near the middle of the fault trace where the slip is relatively high. The fault locally contains multiple strands, each marked by a prominent trough, such as on the east slope of Pear Lake (Fig. 2). Near the westernmost end of the fault trough (at 4050760N, 348572E) the trough extends over a ridge cut by numerous joints that strike N25E. The trough here could be due to concentrated jointing near the fault end (see Segall and Pollard, 1983) rather than marking the end of the actual fault, but dikes offset by ~20 m occur about 670 m to the ENE. We consider the west end of the fault trace to occur in this 670 m interval. The east end of the fault trough (at 4054108N, 355288E) intersects the western right-lateral fault mentioned above; the right-lateral fault is left-laterally deflected at this point. We consider this intersection to effectively mark the east end of the Pear Lake fault.

The Pear Lake fault has a somewhat helicoidal shape.

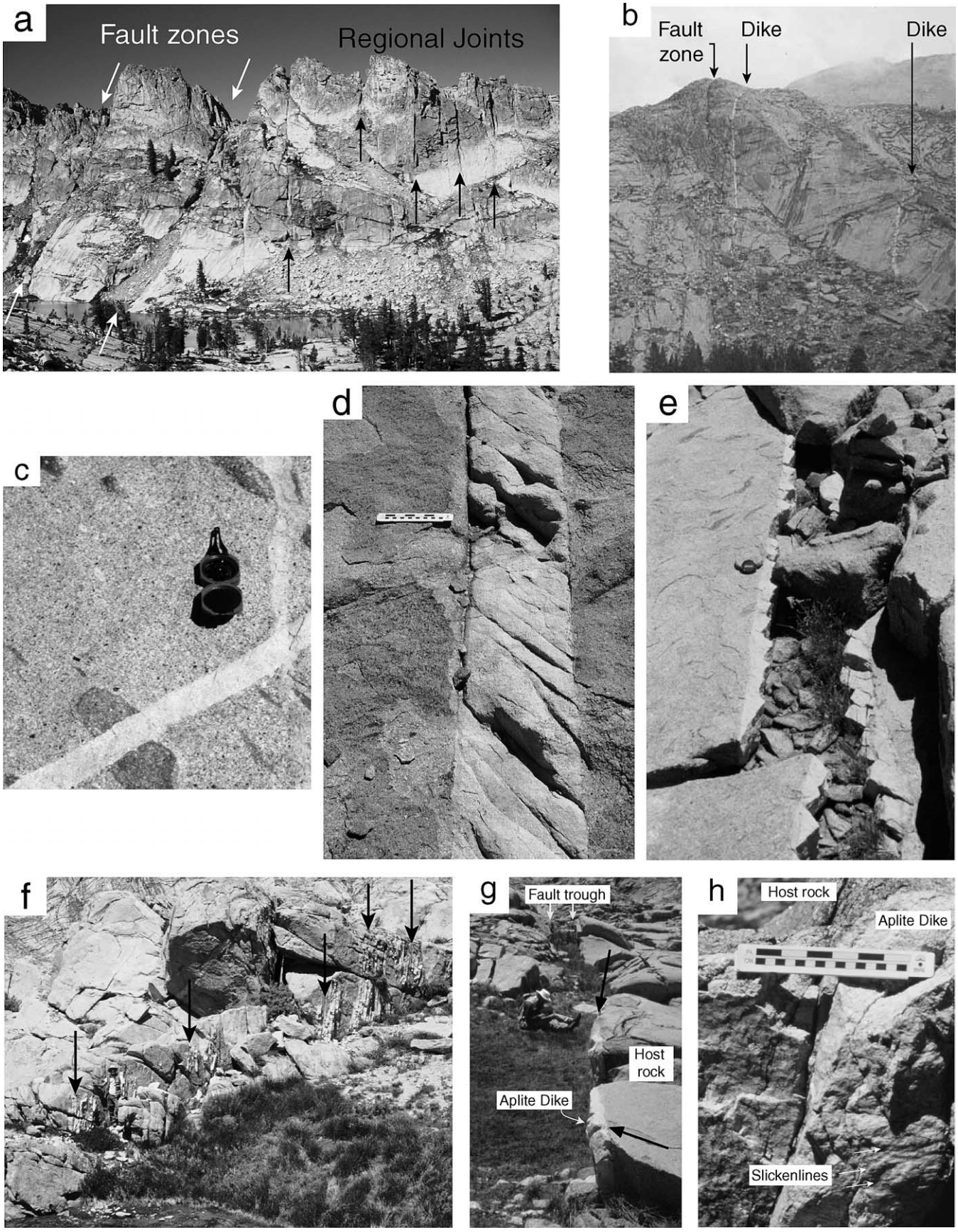
a
Fault zones
Regional Joints
b
Fault zone
Dike
Dike
c
d
e
f
g
Fault trough
Host rock
Aplite Dike
h
Host rock
Aplite Dike
Slickenlines

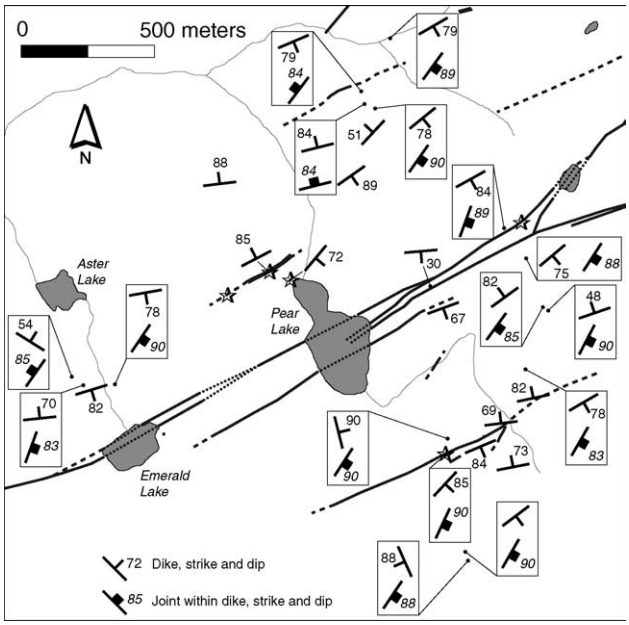

Fig. 6. Map showing attitudes of dikes and of joints in dikes. Stars show where the margin of a fault consists of fractured aplite.

West of the Mitchell Peak Granodiorite, the overall fault strike is N62E and the average dip appears to be about 80° to the south. Solutions to three-point problems yield local strikes ranging between N58E and N65E, and local dips ranging from 63° to the south (on the ridge west of Emerald Lake), to 90° (at Pear Lake). The overall strike of the eastern half of the fault is about N70E, with a dip of about 80° to the north.

Exposures of the internal structure of the fault are rare, but where they occur they are highly fractured. These exposures, coupled with the topographic expression of the fault as a trough, indicate that the rock within the fault is highly fractured throughout. Outcrops within the fault trough consist of green chloritized granitic rock, in places containing pieces of offset aplite dikes. In several areas, outcrop exposure within the trough was good enough that we were able to trace sections of aplite across the trough and map the amount of slip along individual fault structures within the fault core. Typically, the two parallel faults along each margin of the trough accommodate the majority of the slip. For example, at one location (352200E 4052520N on Fig. 2) we mapped three faults in the highly fractured chloritized rock within the fault trough. These had a total of just 3 m of slip, whereas the faults bounding the trough accommodated 41 and 11 m. The chlorite-bearing rock locally contains fine-grained white mica; both minerals indicate that the fault served as a conduit for hydrothermal fluids. In numerous places aplite is exposed along the walls of the fault trough where its contact with the granitic host rock is sharp and parallel to the trough margin (Figs. 5f–h and 6). Aplite along the fault margins typically contains closely spaced fractures that strike ~N25E and dip steeply, consistent with the orientation of regional joints and of joints in unfaulted dikes (Fig. 5f–h). The exposures of the fault interior along with the generally excellent exposures outside the fault provide an opportunity to gain insight into the process of fault formation, allow for precise mapping of the fault zone geometry, and enable detailed measurement of the amount of slip accommodated by the fault.

4. Slip profiles

To prepare slip profiles we collected (a) 'absolute' location data along faults and dikes, and (b) relative location data for offset markers. Absolute locations were found using a combination of GPS instruments, orthophoto images, and aerial photographs. The absolute locations have estimated errors less than 15 m. Relative locations of points on offset markers were measured with an electronic rangefinder, an inclinometer, and pocket transits. The relative locations could be reproduced consistently within 0.1 m.

Evaluating slip along a fault requires determining the relative displacement of pairs of piercing points on opposing walls along the fault. In the field, we identify offset markers such as dikes or other features that are all locally planar and therefore intersect the fault plane as a pair of lines rather than a pair of individual piercing points. To uniquely calculate the slip magnitude, we must know the orientation of the slip vector. We calculate the location of a piercing point by finding the intersection of three planes: the fault, the offset marker, and a plane that intersects the fault in the orientation of the slip vector (Fig. 7). In many places slickenlines or grooves on the fault wall provide evidence for the orientation of the slip vector, but in other places the slip vector must be assumed, as is discussed further below.

Fig. 5. Photographs of joints, faults and dikes near Pear Lake. (a) The Pear Lake fault and regional joints exposed in the ridge west of Pear Lake. The photo was taken looking S30W, approximately parallel to regional joints. The main strand of the fault cuts the ridge at deep notch near the center of the photograph and strikes ENE. The joints strike NNE, oblique to the fault. (b) View to ENE of aplite dikes and a parallel fault zone in a slope 0.5 km north of Pear Lake. (c) View to north of ENE-striking aplite dike (with joints) that cuts an inclusion but does not offset it left-laterally. The ENE-striking aplite dike also appears to cut an aplite dike that strikes to the north. Compass points north. (d) ENE-striking aplite dike with closely spaced échelon joints with photo taken along strike of dike. The joints strike NNE. Note the scarcity of joints in the host rock. The scale is 15 cm long. (e) View to ENE of an exfoliation slab that has broken along a dike with échelon fractures. Note the scarcity of joints in the host rock. (f) View to northeast of fractured aplite (arrows) on the north margin of the Pear Lake fault. This spot is 0.8 km ENE of Pear Lake. (g) View along an ENE-striking fault zone trough showing aplite dike along trough margin. Large black arrows indicate the sharp contact between aplite and host rock. Échelon fractures in the aplite are not easy to see from this perspective, but they do cast shadows near the bottom black arrow. At its narrowest point in the photo, the trough is 66 cm wide. Near UTM coordinates 354610E, 4053285N. (h) Slickenlines on the face of échelon fractures in aplite along the margin of the fault zone trough shown in (g). The slickenlines are located on the planar surface of one of the échelon fractures, indicating that slip occurred after the fractures formed. View is to the north, taken from where the author is seated in (g).

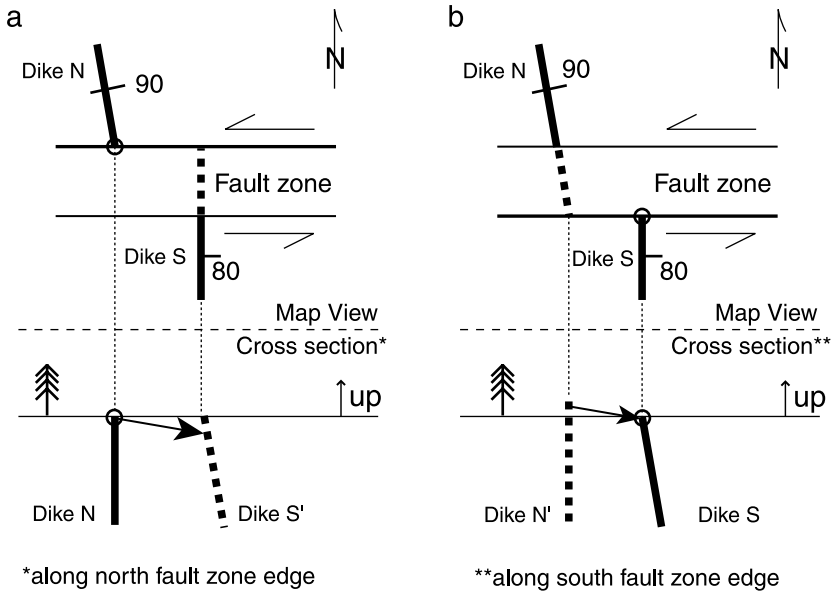

Fig. 7. Diagram showing how slip is evaluated where the orientation of a marker dike differs on opposite sides of a hypothetical fault zone. The figures are orthographic projections with a map view above the horizontal dashed lines and a cross-section below it. The fault is vertical and strikes east. Dikes are shown by the heaviest lines. Dike segment N, on the north side of the fault, strikes N10°W in this example and is vertical. Dike segment S, on the south side of the fault, strikes north in this example and dips 80° to the east. In (a), the reference piercing point is shown by the circle and is set where the dike trace on the north side of the fault (Dike N) intersects the north edge of the fault trace. The cross-section in (a) is taken along the north edge of the fault where Dike S′ is the projection of Dike S across the fault. In (b), the reference piercing point is set where the dike trace on the south side of the fault (Dike S) intersects the south edge of the fault trace. The cross-section is taken along the south edge of the fault, and Dike N′ is the projection of Dike N across the fault. We calculate the slip by connecting a vector with a specified plunge (shown by the arrow) that passes through the reference point and intersects the projection of the dike from the opposite side of the zone. In this example the slip in (a) is about 20% greater than the slip in (b).

This approach yields unique solutions for piercing point locations if (1) the fault is of vanishing thickness, (2) the markers are parallel on the opposing walls of a fault, and (3) fault striations are available. Since these conditions are rarely met precisely, uncertainty is introduced into the calculated slip values. For example, the dikes could be deformed during fault growth or fault slip, and they might not have been perfectly planar to begin with. To account for this complication, for each offset marker we calculate one pair of piercing points on the north edge of the fault zone and a second pair on the south edge. Owing to possible differences in orientation of dike pieces on opposing walls of the fault and to the thickness of the fault zone, the north side and south side piercing-points pairs generally yield somewhat different values of slip across the fault. The error bars in subsequent figures represent the high and low values for slip calculated in the manner described.

Slickenlines provide a gauge as to the inclination of the slip vector, but neither their distribution nor their orientation is uniform. Chloritized slickenlines along the walls of the Pear Lake fault are most common along the eastern half of the fault. They occur on both the granitic host rock and on fractures in the aplite at the fault margins (Fig. 5h). Most of the measured slickenlines have plunges of less than 10°, but some plunge as steeply as 30° (Fig. 8a). Slickenlines plunge to both the ENE and the WSW, with reversals in plunge direction locally occurring over distances of tens of meters or less and therefore cannot be used to uniquely and reliably determine the net slip vector plunge. Based on the slickenlines, we infer that slip is predominantly strike slip. Figure 8c shows the slip distribution along the Pear Lake fault for a horizontal slip vector.

The range in slickenline plunges prompts us to consider how sensitive slip values are to the assumed plunge of the slip vector. Fig. 8d shows calculated slip distributions along the Pear Lake fault for uniform slip plunges of 0°, 10° to the east (+10°), and 10° to the west (−10°). Even for this relatively modest range in plunge values, the calculated slip for markers with shallow dips shows considerable scatter. We find that five slip values, shown with dots in Figs. 8c and d, 9 and 10a, are highly sensitive to the assumed plunge of the slip vector. This reflects the shallow dip of the offset features at those points (in one case as low as 14°). The reader should note that our error bars do not reflect this sensitivity to the plunge of the slip vector. Although we include the slip values plotted with dots for completeness, we consider them suspect. In the discussion that follows we assume that the slip vector is horizontal, so calculated slip values in Fig. 8c are equivalent to horizontal separations (see Ramsay and Huber, 1987).

Figure 8c shows our preferred version of the slip profile for the Pear Lake fault. Overall, the profile shows that peak slip occurs on the western side of the fault at the Alta Peak dike, but there is also a distinct local maximum for the eastern half of the fault. The ratio of peak slip to trace length is 0.01. The outstanding feature of the profile, however, is a

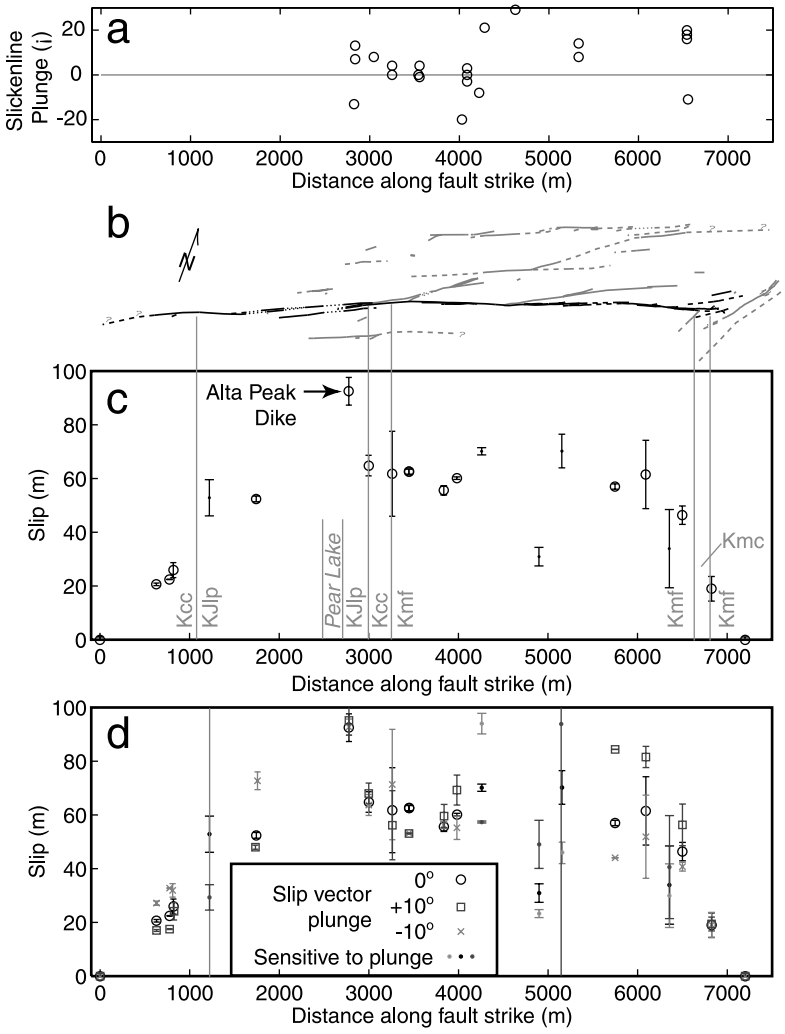

Fig. 8. (a) Observed slickenline plunges along the Pear Lake fault. Plunges to the east are positive, and plunges to the west are negative. The projections of locations here and in Figs. 9 and 10 are onto a plane that strikes N70E. The locations of slickenlines in general do not coincide with places where slip values are calculated. (b) Diagram of fault traces, with traces for the Pear Lake fault shown with the darkest lines. (c) Slip distribution along the Pear Lake fault for a horizontal slip vector. The light gray vertical lines mark contacts and the location of Pear Lake. (d) Calculated slip along the Pear Lake fault for slip vector plunges of 0°, +10° (plunge to east), and −10° (plunge to west). Tiny dots with error bar mark values that are highly sensitive to the assumed slip vector plunge. The values for a plunge of 0° are the same as those shown in (c). The two tallest vertical lines in (d) reflect large error bars.

sharp change in slip immediately east of the Alta Peak dike. The slip drops sharply from a maximum value of 92 m at the dike to ~60 m just 200 m to the east—a drop of 35%. Slip values bracketing the sharp change are reliably constrained. They have low calculated uncertainty and are relatively insensitive to assumptions about the slip vector plunge. A fault branches to the NE off the Pear Lake fault close to where the abrupt drop occurs (Fig. 8b). Our data do not allow us to determine whether this abrupt drop reflects a discontinuity in slip or a steep slip gradient in a continuous slip distribution.

5. Regional stress field during jointing and faulting

The orientation of joints can be used to infer the orientation of the regional principal stresses during the time of jointing (Pollard and Segall, 1987). Steeply dipping regional joints crosscut the granitic foliation and do not seem to be controlled by it. We therefore infer that when the regional joints opened the least compressive stress was horizontal and had a trend of ~N60W, perpendicular to the regional joint strike of ~N30E. We assume that the most compressive horizontal stress was parallel to the joint strike and that the other principal stress was vertical.

Fractures oblique to a fault commonly open during faulting, and they indicate the orientation of the regional principal stresses during faulting (Segall and Pollard, 1980; Martel, 1997; Martel and Boger, 1998). A consistent set of oblique opening mode fractures exists along the margins of faults near Pear Lake. They strike ~N30E and dip steeply, similar to the regional joints, and we do not see systematic fractures of other orientations. We therefore infer that the

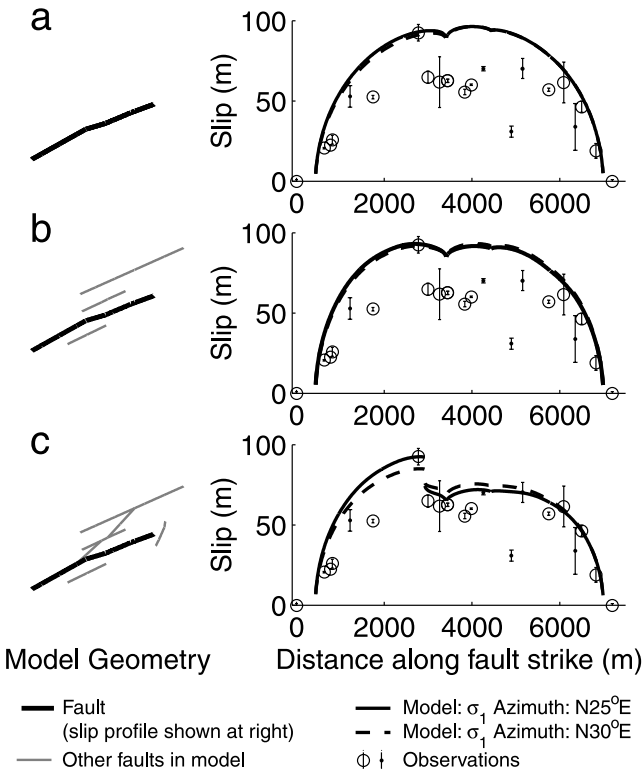

Fig. 9. Comparison between model slip distributions (curves) and observed slip values (symbols with error bars) along the Pear Lake fault for fault networks of increasing complexity. The slip values are found assuming a slip vector plunge of 0° (Fig. 8c). The model fault geometries are in the left column of line drawings, with the Pear Lake fault indicated with the thickest line. Here we only show slip for the Pear Lake fault; see Fig. 10 for slip along other faults. Results are shown for two different trends of the most compressive regional stress: N25E (solid curves) and N30E (dashed curves). Model geometries shown are: (a) an isolated Pear Lake fault with a bend; (b) Pear Lake fault with neighboring ENE-striking faults; and (c) Pear Lake fault with all the major faults we mapped on Fig. 2, including branching faults. Only the model that includes branching faults (c) reproduces the sharp drop in the observed values near 3000 m.

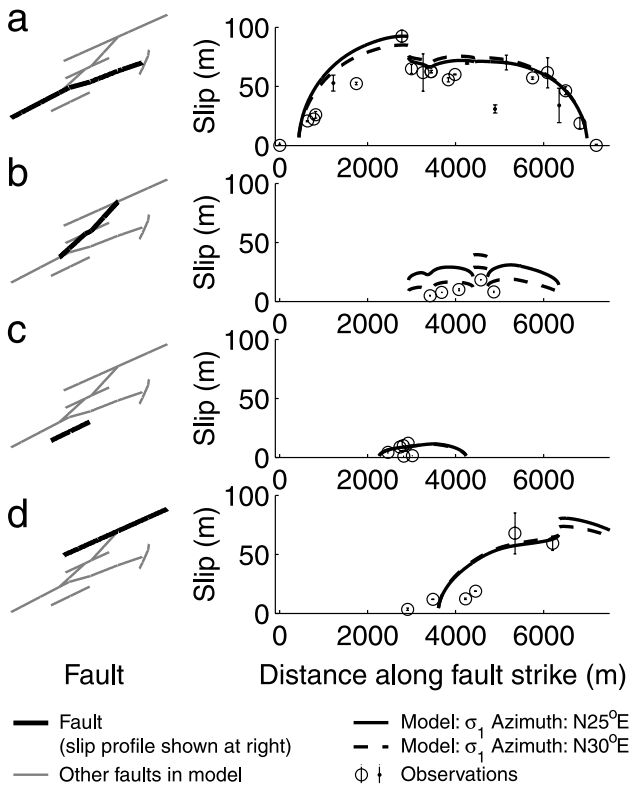

Fig. 10. Comparison between model slip distributions (curves) and observed slip values (symbols with error bars) for faults in the network near Pear Lake. The slip values are found assuming a slip vector plunge of 0°. The slip distribution in the right column is for the fault indicated with the thickest line in the left column. Results are shown for two different trends of the most compressive regional stress: N25E (solid curves) and N30E (dashed curves). Slip profiles are shown for: (a) Pear Lake fault (Fig. 9c); (b) a composite of the 'southern branch fault', central Table Meadows fault, and the 'northern branch fault'; (c) Alta Peak fault; and (d) Kaweah River fault.

orientations of the regional principal stresses during faulting and jointing were essentially the same. This scenario would occur if the faulting and jointing occurred contemporaneously.

The inferred stress field at Pear Lake is consistent with other structural features in the southern Sierra Nevada that formed at a similar time. Faulting at Pear Lake seems to have occurred with the most compressive stress trending NNE–NE, an orientation similar to observations at the well-documented Bear Creek area 90 km to the north (see also Segall and Pollard, 1983). The faulting in the two areas might be contemporaneous and therefore reflect a regional deformation event: the faulting near Pear Lake must be younger than faulted Mitchell Peak Granodiorite, dated at 91 Ma (U–Pb; Chen and Moore, 1982), and the joints and faults at Bear Creek are dated at 79–85 Ma (white mica, K–Ar; Segall et al., 1990; see also Bergbauer and Martel, 1999). Numerous other late Cretaceous plutons between Pear Lake and Bear Creek also developed left-lateral faults that strike ENE. For example, about 19 km NE of Pear Lake, numerous left-lateral faults that strike ENE cut the Paradise Granodiorite. This pluton has yielded dates of 78 Ma (biotite, K–Ar; Evernden and Kistler, 1970), 84 Ma (hornblende, K–Ar; Evernden and Kistler, 1970), and 83–86 Ma (U–Pb; Chen and Moore, 1982). Although the Bear Creek dates seem to rule out the Cenozoic faulting event postulated by Lockwood and Moore (1979), a regional faulting event at 79–85 Ma affecting the southern High Sierra remains a strong possibility. Right-lateral slip at 85 Ma along the proto-Kern Canyon fault (Busby-Spera and Saleeby, 1990), which strikes roughly north–south and is exposed ~17 km east of Pear Lake, is also consistent with this. We have been unable to collect sufficient white mica from the faults near Pear Lake for dating to help test this scenario further.

6. Mechanical analysis

We conducted two-dimensional elastic analyses of slip to aid in understanding (a) the shape of the slip profile for the Pear Lake fault, especially the sharp drop in slip east of

the Alta Peak dike; and (b) the relative values of slip on the faults we mapped. We opted for analyses in two dimensions rather than three dimensions for two main reasons. First, our focus is on slip profile shape and relative slip values along fault strike. Our slip data lend themselves to treating the faults in map view as mode II shear fractures. The fault slip appears to be nearly horizontal, and our data are collected along a roughly horizontal traverse along fault strike (i.e. the elevation range of the data is small compared with the fault trace length). Although a two-dimensional mode II analysis implicitly treats faults as being much taller than they are long, and would overestimate the absolute value of slip, we expect the errors in slip profile shape and in relative slip values to be acceptable. Second, a three-dimensional model would not be well constrained. In particular, our field data constrain neither the relative nor the absolute vertical dimensions of the faults, nor do they constrain fault shape in three dimensions. In light of our objectives and the nature of our data, a two-dimensional analysis seems more appropriate than three-dimensional analyses.

We used a modified version of the boundary element code TWODD (Crouch and Starfield, 1983) in our analyses. We began by defining a model geometry, with the faults considered to be preexisting weaknesses that will slip under an applied shear stress. The model thus focuses on how fault geometry impacts the slip distribution and does not address the initiation of the fault. The faults were modeled with elements about 10 m long. We set all elements to be free of shear tractions; this treats the fault elements as though they were insensitive to the normal traction on them and yields the maximum slip possible. We also required the walls of the faults to remain in contact. The host material is taken to be homogeneous, isotropic, and isothermal. Poisson's ratio was set to 0.25. We imposed a uniform ambient stress field far from the fault and used the boundary element technique to determine the amount of slip required on each element to respond to this stress field, including any local modifications to the stress field due to fault interaction. To get some sense of the sensitivity of our results to the orientation of the principal stresses, we considered two different orientations for the most compressive horizontal stress: N25E and N30E. The magnitudes of the principal stresses and of the shear modulus are arbitrary: we scaled the model results such that they yielded a specified value for the slip at a specified point (e.g. 92 m at the Alta Peak dike).

Fig. 9 shows slip profiles along the Pear Lake fault for three models of increasing complexity. For one fault with a slight bend (Fig. 9a) the profile is nearly elliptical: the profile closely resembles that for an isolated fault with a straight trace. This model fails to produce the abrupt drop in slip slightly east of the Alta Peak dike, and it predicts slip values too high everywhere except at the Alta Peak dike. An isolated fault thus cannot explain the observed slip profile. The results are similar for a model with all four of the major ENE-striking faults within the study area (Fig. 9b). The model that includes the four ENE-striking faults and the other main faults in the area of study clearly fits the data the best and is our preferred model (Fig. 9c). The model slip profile is asymmetric, with local maxima on either side of an abrupt step (discontinuity). The step occurs because slip is split (shared) with a branching fault. This model profile also fits the slip values for the eastern half of the profile well, but it overestimates the slip values in the west. The model slip values in the west would be diminished and have a more linear form if the coarser grained rock of the western part of the profile were modeled as stiffer than the finer grained rock in the eastern part (see Fig. 10c of Bürgmann et al., 1994). The slip values along the Pear Lake fault are matched somewhat better if the most compressive regional stress trends N25E (solid curves) rather than N30E (dashed curves). The results are sufficiently similar though that we hesitate to claim one result is more probable, especially given the simplicity of our model. For a most compressive regional stress trending N35E the model yields local maxima of virtually equal magnitude on the eastern and western halves of the fault and does not produce distinctly lower slip on the eastern half; this result is inconsistent with our slip data. The model that most faithfully reproduces the observed slip on the Pear Lake fault (Fig. 9c) is the one that accounts for all the major observed faults, with the branching faults being particularly important to include. The model slip profile is qualitatively consistent with three-dimensional analyses of branched fault systems (Maerten et al., 1999; Maerten, 2000).

To test the model of Fig. 9c we compared the predicted slip profile with the observed slip along the Pear Lake fault and three of its neighbors (Fig. 10). In Fig. 10, the model slip profiles on all the faults are scaled together such that the peak slip on the Pear Lake fault is 92 m at the Alta Peak dike: the profiles in Fig. 10b–d are not scaled separately. The faults that are the most sensitive to whether the most compressive horizontal stress trends N25E or N30E are the branch faults, which strike northeast, and the Table Meadows fault, to which the branch faults connect. The model matches the slip values on that fault better for a most compressive stress trend of N30E. Both models account for the slip on the Alta Peak fault fairly well (Fig. 10c). For the Kaweah River fault (Fig. 10d) both models over-predict the plotted slip values near the 4000-m-mark by about a factor of two. We do not feel that this misfit invalidates our entire model, for the faulting along the Kaweah River is particularly complicated and it is possible that we either did not measure all the slip across the fault or did not map all faults there. The model also predicts a peak right-lateral slip of $\sim$18 m along the fault at the east end of the Pear Lake fault. We have measured right-lateral separations of 8.5 and 12.7 m across this fault, and a comparable amount of slip seems likely along its neighbor to the east, so the model prediction probably fits the total slip fairly well. We find the overall fit of the model to the data to be remarkably good considering the simplicity of the model.

7. Discussion

7.1. Faults from dikes

Several lines of evidence indicate that the ENE-striking faults near Pear Lake originated from preexisting ENE-striking dikes (Fig. 11). First, the dikes and faults are essentially parallel (Figs. 4 and 5b): they are geometrically related (collocated). Second, in some places aplite dikes that are subparallel to the faults extend into the fault troughs—they coincide spatially (Figs. 5f–h). Third, closely-spaced NNE-striking joints preferentially develop in the dikes (Fig. 5d). The joints weaken the dikes (Fig. 5e) and make them susceptible to shear failure. Fourth, highly fractured aplite forms fault margins at several places (Fig. 5f, g), with joints in the aplite striking ~N25E, the same orientation as in other fractured dikes near the faults. Fifth, and perhaps most important, chloritized slickenlines exist along fractures in fault-margin aplite (Fig. 5h). All these observations are consistent with faulting occurring along the dikes after the dikes were intruded and were fractured. Previous studies have emphasized the role the preexisting joints play in nucleating faults. We conclude that dikes can also play a critical role in fault nucleation, because they can serve to localize fractures.

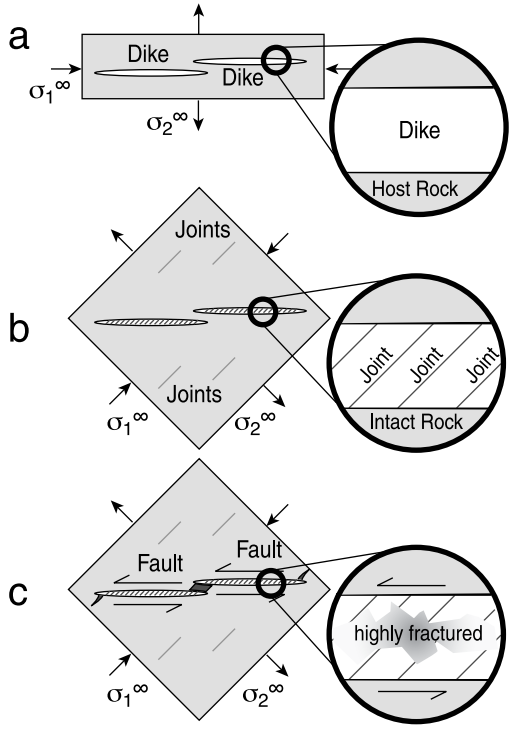

Fig. 11. Cartoon showing evolution of dikes to faults. Insets highlight the role of closely spaced joints within the dikes in this evolution. None of the cartoons are drawn to scale. (a) Intrusion of ENE-striking aplite dikes. (b) Rotation of principal stresses about a vertical axis, with the development of joints striking ~N30E, with joints being particularly concentrated in the ENE-striking aplite dikes. The joint spacing is typically 5–15 cm within fractured dikes at Pear Lake. (c) Failure of highly fractured dikes in shear and formation of faults. As slip accumulates, the dike material is fractured more intensely, making the fault more susceptible to erosion.

Based on our analyses, we have developed a conceptual model for the formation of faults from dikes, as illustrated in Fig. 11. Following intrusion and crystallization of the dikes (Fig. 11a), the principal stresses rotated ~40° counter-clockwise about a vertical axis such that the most compressive horizontal stress was oriented ~N30E. Joints then opened throughout the region but were strongly concentrated in the dikes (Fig. 11b). Eventually the fracturing weakened some dikes sufficiently that they 'tore', failed as shear fractures, and became left-lateral faults.

The two left-lateral faults branch faults strike N35E–N45E and parallel local photolineaments, some regional joints, and some dikes (Figs. 2–4). We infer that those two faults exploited either joints or dikes, or a combination of joints and dikes. Our field observations and mechanical analyses do not allow us to rule out any of these options conclusively. We have not observed highly-fractured dikes that strike parallel to the branch faults though, and this observation seems more consistent with joints playing a larger role than the dikes in the nucleation of the branch faults.

7.2. Implications for the formation of long faults

Scholz (2002) noted that if faults characteristically develop from pre-existing joints, then widespread jointing would seem to be a pre-requisite for the formation of long faults. In fact, few of the mechanisms known for fault growth provide a satisfactory explanation of how long faults form. Our observations show that faults several kilometers long can develop from dikes weakened by concentrated fracturing; this is a previously unrecognized way for faults to develop. We see no reason why dikes could not serve as nuclei for faults much longer than several kilometers. Many dikes attain lengths of tens of kilometers, and dikes in the Mackenzie dike swarm of Canada attain lengths of more than 2000 km (Ernst et al., 2001). Dikes also commonly develop closely spaced fractures during cooling, and hence many dikes form weak narrow zones that would seem ideal for nucleating long faults. While many processes might allow long faults to form in nature, one process is the exploitation of dikes weakened by fractures.

7.3. Comparison with other processes of fault formation

A variety of ways have now been documented by which opening mode fractures serve as nuclei for faults and shear zones. At Pear Lake, aplite dikes are fractured at a macroscopic scale. At Bear Creek, 90 km to the north, strike-slip faults developed from preexisting joints bearing epidote and chlorite (Segall and Pollard, 1983; Martel et al., 1988). During the initial stages of faulting there, crystal plastic deformation occurred in the joint fillings (Segall and

Pollard, 1983), and in some cases this was followed by grain scale fracturing of the filling material (Martel et al., 1988). Crystal plastic deformation also played a role in the nucleation of shear zones along preexisting dikes at Bear Creek (Segall and Simpson, 1986; Christiansen, 1995). Martel and Peterson (1991) showed that foliated metamorphosed mafic dikes in Switzerland evolved into faults, with foliation planes in the metamorphosed dikes accommodating at least some of the slip. These examples illustrate that diverse processes can cause opening-mode fractures to evolve into faults and shear zones.

The process of fault development near Pear Lake also has a parallel in the dolomite of northern Italy. Mollema and Antonellini (1999) concluded that faults in the dolomite developed from bands of échelon joints that subsequently failed in shear. Individual joints in a band are oblique to the band as a whole, and they are inferred to strike parallel to the most compressive horizontal stress. In both our interpretation for Pear Lake and the interpretation of Mollema and Antonellini (1999), the concentration of joints developed contemporaneously with faulting but in the early stages (see also Peacock, 2001). Mollema and Antonellini (1999) noted that some bands coincide locally with veins. If joint bands did exploit veins, then the processes of fault formation in the dolomite would be geometrically and kinematically similar to the process we envision for the faults near Pear Lake.

The fractures observed in the faulted dikes of Pear Lake are geometrically similar to oblique échelon fractures between the bounding faults of simple fault zones of Bear Creek (Martel et al., 1988), but the relative timing of fracturing appears to differ. The fractures within simple fault zones are inferred to develop in the later stages of faulting, whereas we infer that the joints in the dikes of Pear Lake precede the faulting. Also, the joints in the dikes at Pear Lake are essentially fractures within previously filled fractures, whereas the fractures in the simple fault zones are fractures between fractures. Geometric similarity does not guarantee a similar sequence of development.

These examples illustrate many variations on the common theme of opening-mode fractures evolving into faults. Weaknesses or deformation within the filling of the fractures in many cases enable this process. The variations are sufficiently numerous that the common theme can be obscured. An opening mode origin for a fault is also likely to be obscured as a fault becomes larger and accommodates more slip. Based upon observations at Pear Lake and previous work, we suspect that opening mode fractures might have served as nuclei for faults much more commonly than has been previously recognized, a point also noted by Crider and Peacock (2004).

7.4. Control of fault network structure on slip distribution

The key predictions of our mechanical analyses pertain to fault interaction, and in particular interaction effects on slip distribution and peak slip. For example, a sharp change in slip along the Pear Lake fault occurs just east of the Alta Peak dike. Local slip maxima occur on each side of this sharp change. The sharp change and the local slip maxima appear to reflect the effect of the southern branch fault; they might be hallmarks of fault intersections (Maerten et al., 1999; Maerten, 2000). Slip minima and maxima have been interpreted as reflecting points where faults cut barriers or where they nucleate (Ellis and Dunlap, 1988; Manighetti et al., 2001). Our results show that local minima and maxima in slip can also be associated with a branched fault structure. The predicted peak slip on the Table Meadows fault already exceeds the measured value, but additional calculations show that the predicted peak would have been 10–30% higher if the Pear Lake fault were not accounted for. Similarly, the predicted peak slip of 18 m on the right lateral fault at the east edge of the study area is close to the observed value, but the predicted peak would have been 2–3 times smaller if the Pear Lake fault were not accounted for. The spatial distribution of the faults thus affects the distribution of slip on the faults (e.g. Schultz, 1999; Gupta and Scholz, 2000). The sense of slip on the faults experiencing a most compressive horizontal stress trend of N30E could have been predicted based on just the orientation of the faults, but to understand the distribution of slip and the peak values of slip the positions and dimensions of the faults need to be considered. The distribution of structures that preceded the faulting (i.e. dikes and joints) control to a large extent the fault network geometry and hence the ultimate slip distribution.

7.5. Implications for scaling

Scaling of faults commonly is discussed in terms of trace length (e.g. Walsh and Watterson, 1988). Trace length information can be used, among other things, in stochastic analyses of fault hydraulic behavior or, when coupled with data on maximum slip, in estimating regional strain (e.g. Walsh et al., 1991). Even for a single parallel set of faults, however, the slip will not depend just on the fault trace length scale, but on a host of other factors (e.g. Bürgmann et al., 1994; Willemse et al., 1996; Schultz, 1999), including fault spacing scales. For faults that form by exploiting preexisting joints or dikes that spacing scale can vary significantly. For example, Segall and Pollard (1983) and Segall (1984) show jointed outcrops in the Sierra where the representative spacing of joints is several centimeters, or about two orders of magnitude less than the typical trace length. Near Pear Lake the typical trace length scale of dikes is on the order of hundreds of meters, yet the typical spacing is tens to hundreds of meters, about one order of magnitude less. One would expect faults that developed from joints to have a different spacing of steps and bends than faults that developed from dikes. In an area such as that near Pear Lake, where faults exploit a mix of structures with different orientations, the faulting is likely to be more complex, with a variety of length scales being present. The variety of

length scales affects the distribution of fault intersections, and hence the slip behavior of a system of faults and the hydraulic behavior (National Research Council, 1996). Lithologic variation will introduce additional length scales that affect fracture dimensions, such as bedding thickness and formation thickness. In addition, because the faulting process introduces new fractures and new linkages, the distribution of length scales will change with time. Simple scaling relationships based on trace length may be useful in revealing general trends, but analyses of the type presented here, which account for the geometry, history, kinematics, and mechanics of a fault system should provide substantially more insight into fault system behavior.

8. Conclusions

The central finding of our study is that faults several kilometers long near Pear Lake nucleated from preexisting highly-fractured dikes. Like joints, dikes are opening mode structures and are nearly planar, but unlike joints, dikes can attain lengths of thousands of kilometers. Distributions of joints that extend great distances along strike thus are not required for the formation of long, roughly planar faults. Long dikes can serve as nuclei for long faults. Others have recognized that dikes can serve as nuclei for shear zones, but to our knowledge the recognition that dikes can evolve into faults by preferential fracturing of dikes is new. Our findings, coupled with a review of the literature, suggest that opening mode fractures might serve more commonly as nuclei for faults than is generally appreciated.

The second key finding is that a network of intersecting faults exists near Pear Lake, and that the slip distributions on the faults reflect their mechanical interaction with each other. The sharp drop in slip along the Pear Lake fault just west of the Alta Peak dike is consistent with fault branching. For models that neglect the Pear Lake fault, the predicted slip on other faults in the study area differs substantially from the observed slip. The distribution of structures that preceded the faulting (i.e. dikes and joints) control to a large extent the fault network structure and hence the ultimate slip distribution on faults in the network. The presence of preexisting flaws of multiple orientations will influence not only the slip distribution of faults, but also their hydraulic behavior. Analyses such as the one here that account for the geometry, history, kinematics, and mechanics of a fault system should provide substantially more insight into fault system behavior than analyses that do not account for all these factors.

Acknowledgements

We thank David Peacock and Emanuel Willemse for their review comments, which resulted in substantial improvements in the manuscript. We gratefully acknowledge support from the U.S. Department of Energy Office of Basic Energy Sciences (Grant No. DE-FG03-85ER14525). This is SOEST contribution #6253.

References

Adams, M., Sines, G., 1978. Crack extension from flaws in a brittle material subjected to compression. Tectonophysics 49, 97–118.

Ague, J.J., Brimhall, G.H., 1988. Magmatic arc asymmetry and distribution of anomalous plutonic belts in the batholiths of California—effects of assimilation, crustal thickness, and depth of crystallization. Geological Society of America Bulletin 100, 912–927.

Bergbauer, S., Martel, S.J., 1999. Formation of joints in cooling plutons. Journal of Structural Geology 21, 821–835.

Brace, W.F., Bombalakis, E.G., 1963. A note on brittle crack growth in compression. Journal of Geophysical Research 68, 3709–3713.

Bürgmann, R., Pollard, D.D., 1994. Strain accommodation about strike-slip fault discontinuities in granitic rock under brittle-to-ductile conditions. Journal of Structural Geology 16, 1655–1674.

Bürgmann, R., Pollard, D.D., Martel, S.J., 1994. Slip distributions on faults: effects of stress gradients, inelastic deformation, heterogeneous host-rock stiffness, and fault interaction. Journal of Structural Geology 16, 1675–1690.

Busby-Spera, C.J., 1983. Paleogeographic reconstruction of a submarine volcanic center; geochronology, volcanology and sedimentology of the Mineral King roof pendant, Sierra Nevada, California. Ph.D. thesis, Princeton University.

Busby-Spera, C.J., Saleeby, J.B., 1990. Intraarc strike-slip-fault exposed at batholithic levels in the southern Sierra-Nevada, California. Geology 18, 255–259.

Chen, J.H., Moore, J.G., 1982. Uranium–lead isotopic ages from the Sierra-Nevada batholith, California. Journal of Geophysical Research 87, 4761–4784.

Christiansen, P.P., 1995. Faulting and hydrothermal processes in a granitic batholith. Ph.D. thesis, Stanford University.

Crider, J.G., Peacock, D.C.P., 2004. Initiation of brittle faults in the upper crust: a review of field observations. Journal of Structural Geology 26, 691–707.

Crouch, S.L., Starfield, A.M., 1983. Boundary Element Methods in Solid Mechanics. Allen and Unwin, London.

Ellis, M.A., Dunlap, W.J., 1988. Displacement variations along thrust faults: implications for the development of large faults. Journal of Structural Geology 10, 183–192.

Ernst, R.E., Grosfils, E.B., Mege, D., 2001. Giant dike swarms: Earth, Venus, and Mars. Annual Review of Earth and Planetary Sciences 29, 489–534.

Evernden, J.F., Kistler, R.W., 1970. Chronology and emplacement of Mesozoic batholithic complexes in California and western Nevada. U.S. Geological Survey Professional Paper 623, 1–42.

Fowler, T.K., Paterson, S.R., 1997. Timing and nature of magmatic fabrics from structural relations around stoped blocks. Journal of Structural Geology 19, 209–224.

Gupta, A., Scholz, C.H., 2000. A model of normal fault interaction based on observations and theory. Journal of Structural Geology 22, 865–879.

Lockwood, J.P., Lydon, P.A., 1975. Geologic map of the Mount Abbot quadrangle, California. U.S. Geological Survey Quadrangle Map GQ-1155, scale 1:62,500.

Lockwood, J.P., Moore, J.G., 1979. Regional deformation of the Sierra Nevada, California, on conjugate microfault sets. Journal of Geophysical Research 84, 6041–6049.

Maerten, L., 2000. Variation in slip on intersecting normal faults: implications for paleostress inversion. Journal of Geophysical Research 105, 25553–25565.

Maerten, L., Willemse, E.J.M., Pollard, D.D., Rawnsley, K., 1999. Slip distributions on intersecting normal faults. Journal of Structural Geology 21, 259–271.

Manighetti, I., King, G.C.P., Gaudemer, Y., Scholz, C.H., Doubre, C., 2001. Slip accumulation and lateral propagation of active normal faults in Afar. Journal of Geophysical Research 106, 13667–13696.

Martel, S.J., 1990. Formation of compound strike-slip fault zones, Mount Abbot quadrangle, California. Journal of Structural Geology 12, 869–882.

Martel, S.J., 1997. Effects of cohesive zones on small faults and implications for secondary fracturing and trace geometry. Journal of Structural Geology 19, 835–847.

Martel, S.J., Boger, W.A., 1998. Geometry and mechanics of secondary fracturing around small three-dimensional faults in granitic rock. Journal of Geophysical Research 103, 21299–21314.

Martel, S.J., Peterson, J.E., 1991. Interdisciplinary characterization of fracture systems at the US/BK Site, Grimsel-Laboratory, Switzerland. International Journal of Rock Mechanics and Mining Sciences & Geomechanics Abstracts 28, 295–323.

Martel, S.J., Pollard, D.D., Segall, P., 1988. Development of simple fault zones in granitic rock, Mount Abbot quadrangle, Sierra Nevada, California. Geological Society of America Bulletin 100, 1451–1465.

Mollema, P.N., Antonellini, M., 1999. Development of strike-slip faults in the dolomites of the Sella Group, northern Italy. Journal of Structural Geology 21, 273–292.

Moore, J.G., Sisson, T.W., 1987. Geologic map of the Triple Divide Peak quadrangle, Tulare County, California. U.S. Geological Survey Quadrangle Map GQ-1636, scale 1:62,500.

National Research Council, 1996. Anon., 1996. Rock Fractures and Fluid Flow: Contemporary Understanding and Applications. National Academy of Sciences, Washington, DC.

Pachell, M.A., Evans, J.P., 2002. Growth, linkage, and termination processes of a 10-km-long strike-slip fault in jointed granite: the Gemini fault zone, Sierra Nevada, California. Journal of Structural Geology 24, 1903–1924.

Peacock, D.C.P., 2001. The temporal relationship between joints and faults. Journal of Structural Geology 23, 329–341.

Pollard, D.D., Segall, P., 1987. Theoretical displacements and stresses near fractures in rocks: with applications to faults, joints, veins, dikes, and solution surfaces, in: Atkinson, B.K. (Ed.), Fracture Mechanics of Rocks. Academic, San Diego, California, pp. 277–349.

Ramsay, J.G., Huber, M.I., 1987. The Techniques of Modern Structural Geology. Volume 2: Folds and Fractures. Academic Press, London.

Scholz, C.H., 2002. The Mechanics of Earthquakes and Faulting. Cambridge University Press, Cambridge.

Schultz, R.A., 1999. Understanding the process of faulting: selected challenges and opportunities at the edge of the 21st century. Journal of Structural Geology 21, 985–993.

Segall, P., 1984. Formation and growth of extensional fracture sets. Geological Society of America Bulletin 95, 454–462.

Segall, P., Pollard, D.D., 1980. Mechanics of discontinuous faults. Journal of Geophysical Research 85, 4337–4350.

Segall, P., Pollard, D.D., 1983. Nucleation and growth of strike slip faults in granite. Journal of Geophysical Research 88, 555–568.

Segall, P., Simpson, C., 1986. Nucleation of ductile shear zones on dilatant fractures. Geology 14, 56–59.

Segall, P., McKee, E.H., Martel, S.J., Turrin, B.D., 1990. Late Cretaceous age of fractures in the Sierra Nevada batholith, California. Geology 18, 1248–1251.

Walsh, J.J., Watterson, J., 1988. Analysis of relationship between displacements and dimensions of faults. Journal of Structural Geology 10, 237–247.

Walsh, J.J., Watterson, J., Yielding, G., 1991. The importance of small-scale faulting in regional extension. Nature 351, 391–393.

Willemse, E.J.M., Pollard, D.D., Aydin, A., 1996. Three-dimensional analyses of slip distributions on normal fault arrays with consequences for fault scaling. Journal of Structural Geology 18, 295–309.